Smoothing methods comparison for CMB E- and B-mode separation

Yi-Fan Wang, Kai Wang and Wen Zhao

CAS Key Laboratory for Research in Galaxies and Cosmology, Department of Astronomy, University of Science and Technology of China, Hefei 230026, China; *ljwk@mail.ustc.edu.cn*

Abstract The anisotropies of the B-mode polarization in the cosmic microwave background radiation play a crucial role in the study of the very early Universe. However, in real observations, a mixture of the E-mode and B-mode can be caused by partial sky surveys, which must be separated before being applied to a cosmological explanation. The separation method developed by Smith (2006) has been widely adopted, where the edge of the top-hat mask should be smoothed to avoid numerical errors. In this paper, we compare three different smoothing methods and investigate leakage residuals of the E-B mixture. We find that, if less information loss is needed and a smaller region is smoothed in the analysis, the sin- and cos-smoothing methods are better. However, if we need a cleanly constructed B-mode map, the larger region around the mask edge should be smoothed. In this case, the *Gaussian*-smoothing method becomes much better. In addition, we find that the leakage caused by numerical errors in the *Gaussian*-smoothing method is mostly concentrated in two bands, which is quite easy to reduce for further E-B separations.

Key words: cosmic microwave background radiation — polarization — statistics

1 INTRODUCTION

Cosmic microwave background (CMB) radiation encoded fruitful information related to modern cosmology, which plays a crucial role for the determination of cosmological parameters (Planck Collaboration et al. 2015). The fluctuations of CMB include three parts: the temperature anisotropies, the E-mode polarization and the B-mode polarization. By precise observations with the WMAP and Planck satellites, CMB temperature anisotropies, E-mode polarization and their correlation power spectra have been well observed (Planck Collaboration et al. 2015). However, the detection of B-mode is still quite poor (BICEP2/Keck and Planck Collaborations et al. 2015; Ade et al. 2014; Naess et al. 2014; Hanson et al. 2013), therefore improving this is the main goal of the next generation of experiments (Bock et al. 2006). In the standard model, the CMB B-mode can only be generated by primordial gravitational waves and cosmic weak lensing (second order effect). So, it provides a unique opportunity to directly probe the physics of the very early Universe through primordial gravitational waves (Kamionkowski et al. 1997a; Seljak & Zaldarriaga 1997).

Compared to the CMB temperature anisotropies and the E-mode polarization, the amplitude of the B-mode polarization is much smaller. Its detection is limited by various contaminations, including foreground radiation, instrumental noise, instrumental systematics and the E-B mixtures due to partial sky surveys (Bock et al. 2006). In this paper, we shall focus on the problem of E-B mixtures. Numerous numerical methods have been developed

to separate E- and B-mode polarization from observable Q and U polarization maps. Among them, the methods developed by Smith & Zaldarriaga (SZ method) (Smith 2006; Smith & Zaldarriaga 2007), Zhao & Baskaran (ZB method) (Zhao & Baskaran 2010), and Kim & Naselsky (KN method) (Kim & Naselsky 2010) have used the so-called χ-field framework, and can be effectively applied to potential data analysis or numerical simulations. In each method, in order to reduce numerical errors, the usual top-hat CMB masks should be replaced by smoothed masks, where the edges of the masks are smoothly joined. In this work, we will compare three different smoothing methods adopted in different literature, and investigate the residuals of the E-B mixtures in those three methods. By this comparison, we will search for the best smoothing method, which induces the smallest leakage in E-B separation.

2 STANDARD PROCEDURE FOR E- AND B-MODE SEPARATION AND PURE PSEUDO-C_l METHOD

First we present a brief review of two related definitions of E- and B-mode. Since CMB polarization does not contain a circular polarization component, it can be completely characterized by Stokes parameters Q and U (Kamionkowski et al. 1997b). We can introduce the complex conjugate polarization fields $P_\pm$ defined as follows

$$P_\pm(\hat{n}) \equiv Q(\hat{n}) \pm iU(\hat{n}),\qquad(1)$$

where $\hat{n}$ denotes the direction of a 2-dimensional sphere. It can be proved that the fields $P_\pm$ have spin of ± 2, which

means that when we rotate the coordinate system by an arbitrary angle α in the plane perpendicular to direction $\hat{n}$, the polarization fields would change as

$$P'_{\pm}(\hat{n}) = P_{\pm}(\hat{n}) \, e^{\mp 2i\alpha}. \tag{2}$$

It is easier to study a scalar field rather than a spin-weighted field. One can construct such electric type and magnetic type scalar fields through Fourier expansion of $P_{\pm}$ and a recombination of expansion coefficients. Expanding $P_{\pm}$ over a basis of spin-weighted spherical harmonic functions gives (Zaldarriaga & Seljak 1997)

$$P_{\pm}(\hat{n}) = \sum_{lm} a_{\pm 2,lm} \, {}_{\pm 2}Y_{lm}(\hat{n}), \tag{3}$$

where ${}_{\pm 2}Y_{lm}$ are ± 2 spin-weighted spherical harmonic functions. One can also calculate multipole coefficients $a_{\pm 2,lm}$ as

$$a_{\pm 2,lm} = \int d\hat{n} P_{\pm}(\hat{n}) \, {}_{\pm 2}Y^*_{lm}(\hat{n}). \tag{4}$$

The coefficients of scalar E and B fields are defined as a recombination of $a_{\pm 2,lm}$

$$E_{lm} \equiv -\frac{1}{2}[a_{2,lm} + a_{-2,lm}],$$

$$B_{lm} \equiv -\frac{1}{2i}[a_{2,lm} - a_{-2,lm}]. \tag{5}$$

Then the E- and B-mode of the polarization field are defined as,

$$E(\hat{n}) \equiv \sum_{lm} E_{lm}Y_{lm}(\hat{n}), \qquad B(\hat{n}) \equiv \sum_{lm} B_{lm}Y_{lm}(\hat{n}), \tag{6}$$

and their associated power spectra are defined as,

$$C_l^{EE} \equiv \frac{1}{2l+1} \sum_m \langle E_{lm}E^*_{lm} \rangle,$$

$$C_l^{BB} \equiv \frac{1}{2l+1} \sum_m \langle B_{lm}B^*_{lm} \rangle, \tag{7}$$

where the brackets denote the ensemble average. Since the E and B fields are Gaussian random fields, the power spectra defined above encode all the statistical information about the fields.

Another related definition is to use spin lowering and raising operators to construct electric type and magnetic type scalar fields (Zaldarriaga & Seljak 1997)

$$\mathcal{E}(\hat{n}) \equiv -\frac{1}{2}[\bar{\eth}\bar{\eth}P_+(\hat{n}) + \eth\eth P_-(\hat{n})], \tag{8}$$

$$\mathcal{B}(\hat{n}) \equiv -\frac{1}{2i}[\bar{\eth}\bar{\eth}P_+(\hat{n}) - \eth\eth P_-(\hat{n})]. \tag{9}$$

$\bar{\eth}$ and $\eth$ are the spin lowering and raising operators respectively, which are defined as follows

$$\bar{\eth}f \equiv -\sin^{-s}\theta \left(\frac{\partial}{\partial\theta} - \frac{i}{\sin\theta}\frac{\partial}{\partial\phi} \right)(f\sin^s\theta), \tag{10}$$

$$\eth f \equiv -\sin^s\theta \left(\frac{\partial}{\partial\theta} + \frac{i}{\sin\theta}\frac{\partial}{\partial\phi} \right)(f\sin^{-s}\theta), \tag{11}$$

where f is an arbitrary function with spin s.

We can decompose the $\mathcal{E}$ and $\mathcal{B}$ fields over the basis of scalar spherical harmonics

$$\mathcal{E}(\hat{n}) \equiv \sum_{lm} \mathcal{E}_{lm}Y_{lm}(\hat{n}), \qquad \mathcal{B}(\hat{n}) \equiv \sum_{lm} \mathcal{B}_{lm}Y_{lm}(\hat{n}), \tag{12}$$

where the decomposition coefficients are calculated as

$$\mathcal{E}_{lm} = \int d\hat{n}\mathcal{E}(\hat{n})Y^*_{lm}(\hat{n}), \qquad \mathcal{B}_{lm} = \int d\hat{n}\mathcal{B}(\hat{n})Y^*_{lm}(\hat{n}). \tag{13}$$

We can construct the power spectra in the same manner as the former method

$$C_l^{\mathcal{E}\mathcal{E}} \equiv \frac{1}{2l+1} \sum_m \langle \mathcal{E}_{lm}\mathcal{E}^*_{lm} \rangle,$$

$$C_l^{\mathcal{B}\mathcal{B}} \equiv \frac{1}{2l+1} \sum_m \langle \mathcal{B}_{lm}\mathcal{B}^*_{lm} \rangle. \tag{14}$$

Thanks to a property of spin lowering and raising operators

$$\bar{\eth}\,{}_sY_{lm}(\hat{n}) = -\sqrt{(l+s)(l-s+1)}\,{}_{s-1}Y_{lm}(\hat{n}),$$

$$\eth\,{}_sY_{lm}(\hat{n}) = \sqrt{(l-s)(l+s+1)}\,{}_{s+1}Y_{lm}(\hat{n}), \tag{15}$$

the relationships of the multipoles and power spectra between these two definitions are

$$\mathcal{E}_{lm} = N_{l,2}E_{lm}, \qquad \mathcal{B}_{lm} = N_{l,2}B_{lm}, \tag{16}$$

$$C_l^{\mathcal{EE}} = N_{l,2}^2 C_l^{EE}, \qquad C_l^{\mathcal{BB}} = N_{l,2}^2 C_l^{BB}, \tag{17}$$

where $N_{l,s} = \sqrt{(l+s)!/(l-s)!}$.

In the actual observation, we must mask out a fractional portion of sky due to foreground contamination. The observed values of Stokes parameters $\tilde{Q}$ and $\tilde{U}$ are related to the real values Q and U by introducing a window function $W(\hat{n})$

$$\tilde{Q} = QW, \qquad \tilde{U} = UW. \tag{18}$$

The value of W is only non-zero in the observed region of sky.

However, if one applies $\tilde{P}_\pm = \tilde{Q} \pm i\tilde{U}$ directly to the above two definitions of the E- and B-mode, it will lead to the so-called E-B mixture problem arising from the cut-sky effect (Lewis et al. 2002; Bunn et al. 2003), dramatically restricting the detectability of the B-mode signal. Several methods were proposed to solve this problem (Lewis 2003; Lewis et al. 2002; Bunn et al. 2003; Bunn 2008; Grain et al. 2009; Smith 2006; Smith & Zaldarriaga 2007; Geller et al. 2008; Cao & Fang 2009; Zhao & Baskaran 2010; Kim & Naselsky 2010). We notice that the article Ferté et al. (2013) has compared three different methods which are numerically fast enough (Smith 2006; Smith & Zaldarriaga 2007; Zhao & Baskaran 2010; Kim & Naselsky 2010) and drew the conclusion that the SZ method (Smith 2006; Smith & Zaldarriaga 2007) is the best from the perspective of significantly reducing E to B leakage and ensuring the smallest error bars at the same time. Therefore we choose to apply this best method to the E- and B-mode separating operation in the following description.

We briefly review how the SZ method separates the E- and B-mode on an incomplete sky. First the concept of pure pseudo-multipoles is put forward and defined as

$$\mathcal{E}_{lm}^{\text{pure}} \equiv -\frac{1}{2} \int d\hat{n} \Big\{ P_+(\hat{n}) \left[\bar{\eth}\bar{\eth}\left(W(\hat{n})Y_{lm}(\hat{n}) \right) \right]^* + P_-(\hat{n}) \left[\eth\eth\left(W(\hat{n})Y_{lm}(\hat{n}) \right) \right]^* \Big\},$$

$$\mathcal{B}_{lm}^{\text{pure}} \equiv -\frac{1}{2i} \int d\hat{n} \Big\{ P_+(\hat{n}) \left[\bar{\eth}\bar{\eth}\left(W(\hat{n})Y_{lm}(\hat{n}) \right) \right]^* - P_-(\hat{n}) \left[\eth\eth\left(W(\hat{n})Y_{lm}(\hat{n}) \right) \right]^* \Big\}. \tag{19}$$

Recall the definition of pseudo-multipoles which are concentrated in the pseudo-C_l estimator technique (Efstathiou 2004)

$$\tilde{\mathcal{E}}_{lm} \equiv \int d\hat{n}\mathcal{E}(\hat{n})W(\hat{n})Y_{lm}^*(\hat{n}), \qquad \tilde{\mathcal{B}}_{lm} \equiv \int d\hat{n}\mathcal{B}(\hat{n})W(\hat{n})Y_{lm}^*(\hat{n}). \tag{20}$$

It can be proved (Smith & Zaldarriaga 2007) that the expressions of Equation (19) and Equation (20) are equivalent. This shows that, in principle, the pure pseudo-multipole method can successfully extract the pure E- and B-mode signal and avoid the E-B mixing part. To calculate the expression of Equation (19), one needs to use the property of spin raising and lowering operators

$$\bar{\eth}(fg) = \left(\bar{\eth}f \right) g + f \left(\bar{\eth}g \right), \qquad \eth(fg) = \left(\eth f \right) g + f \left(\eth g \right), \tag{21}$$

where f and g are arbitrary spin-weighted functions with spin s_1 and s_2, and fg is a spin $s_1 + s_2$ weighted function, together with the complex conjugate relationship $\eth^* = \bar{\eth}$.

Using Equations (15) and (21), and substituting them into Equation (19), one finally obtains (only focusing on the B-mode)

$$\mathcal{B}_{lm}^{\text{pure}} = -\frac{1}{2i} \int d\hat{n} \Big[P_+ \Big((\bar{\eth}\bar{\eth}W)Y_{lm}^* + 2N_{l,1}(\bar{\eth}W)(_1 Y_{lm}^*) + N_{l,2}W(_2 Y_{lm}^*) \Big)$$
$$- P_- \Big((\eth\eth W)Y_{lm}^* - 2N_{l,1}(\eth W)(_{-1} Y_{lm}^*) + N_{l,2}W(_{-2} Y_{lm}^*) \Big) \Big], \tag{22}$$

where

$$\eth W = -\frac{\partial W}{\partial \theta} - \frac{i}{\sin\theta}\frac{\partial W}{\partial \phi}, \tag{23}$$

$$\eth\eth W = -\cot\theta\frac{\partial W}{\partial \theta} + \frac{\partial^2 W}{\partial \theta^2} - \frac{1}{\sin^2\theta}\frac{\partial^2 W}{\partial \phi^2} - \frac{2i\cot\theta}{\sin\theta}\frac{\partial W}{\partial \phi} + \frac{2i}{\sin\theta}\frac{\partial^2 W}{\partial \theta \partial \phi}. \tag{24}$$

Equation (22) is the basis for all following E- and B-mode separating operations.
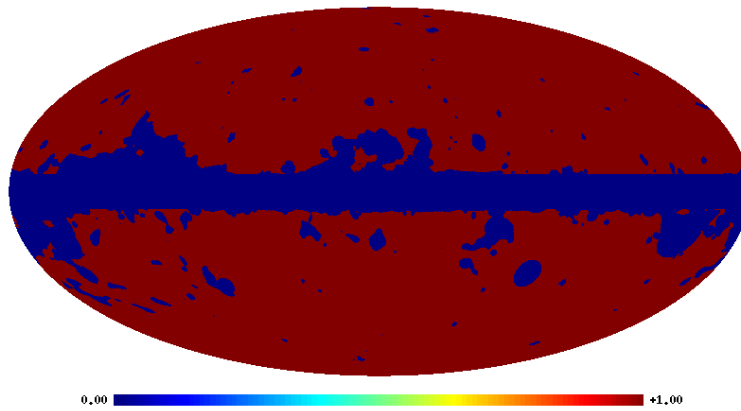
Fig. 1 A window function for CMB polarization published by the Planck Collaboration.
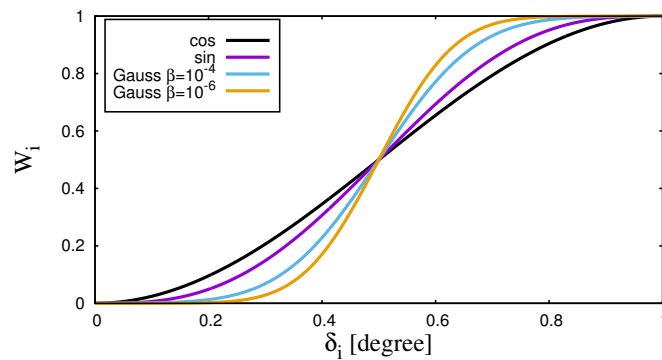
Fig. 2 The plot of cos-smoothing, sin-smoothing and *Gaussian*-smoothing in real space.
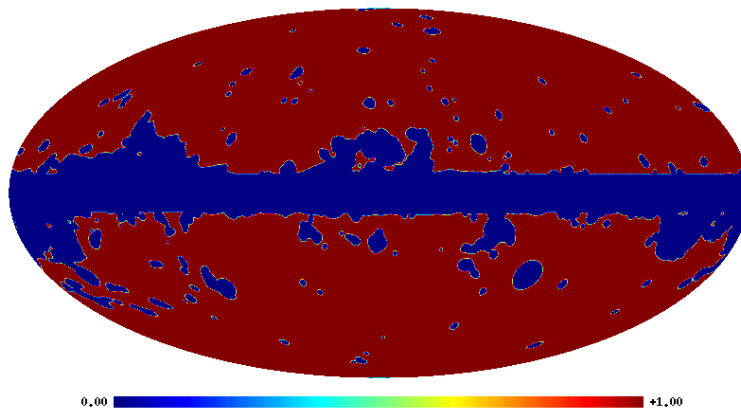
Fig. 3 A smoothed window function using the *Gauss*-smoothing method with parameters $\delta_c = 1°$ and $\beta = 10^{-4}$.

3 SMOOTHING METHODS COMPARISON

In this section we shall discuss the effect on E- and B-mode separation caused by a different choice of window function $W(\hat{n})$. The simplest case is $W(\hat{n}) = 1$ in the observed region of sky and $W(\hat{n}) = 0$ outside (referred to as a "top-hat window function") as shown in Figure 1 published by the Planck Collaboration. However, in Equation (22), the calculation of the derivative of $W(\hat{n})$

is inevitable, so we must smooth the edge of $W(\hat{n})$ (also called "apodization"). The notable point is that the zero-value pixels of the original window function should be zero after being smoothed. Another restriction on the smoothing method of $W(\hat{n})$ given by the SZ method (Smith 2006) is that both W and its gradient should vanish at the boundary of the observed sky. We compare three different smoothing methods for the window functions, which have appeared in the literature and satisfy the above conditions. The first two
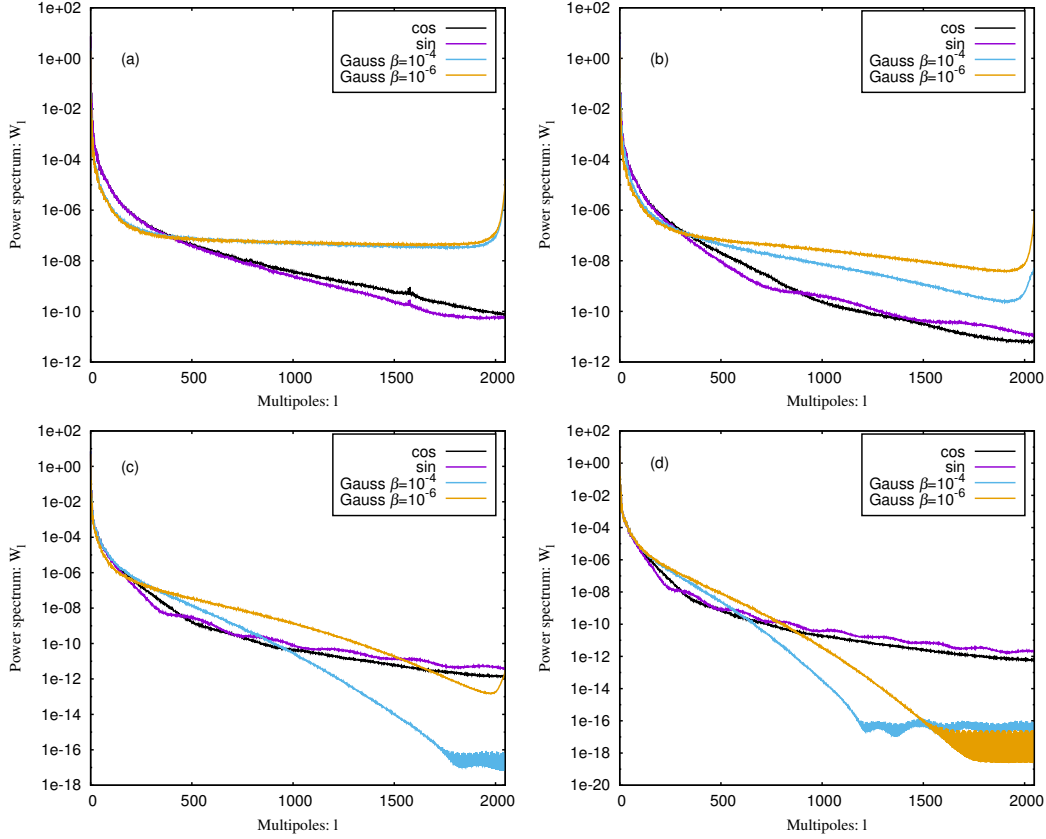
Fig. 4 The power spectrum of smoothing window function $W(\hat{n})$ with different smoothing methods and different parameters. (a) $\delta_c = 0.2°$; (b) $\delta_c = 0.5°$; (c) $\delta_c = 1.0°$; (d) $\delta_c = 1.5°$.

methods use a trigonometric function to smooth the edge of the top-hat window function, referred to as cos-smoothing and sin-smoothing (Grain et al. 2009) respectively. Their expressions are

$$
W_i = \begin{cases} \dfrac{1}{2} - \dfrac{1}{2}\cos(\dfrac{\delta_i}{\delta_c}\pi) & \delta_i < \delta_c, \\ 1 & \delta_i > \delta_c, \end{cases} \tag{25}
$$

and

$$
W_i = \begin{cases} -\dfrac{1}{2\pi}\sin\left(2\pi\dfrac{\delta_i}{\delta_c}\right) + \dfrac{\delta_i}{\delta_c} & \delta_i < \delta_c, \\ 1 & \delta_i > \delta_c, \end{cases} \tag{26}
$$

where δ_i is the distance from each 1-valued pixel to the closest 0-valued pixel in the top-hat window function, and δ_c is a constant set in advance representing the smoothing range.

The third smoothing method is put forward by Kim (2011). This article theoretically analyzed the generation of numerical error in E- and B-mode separation by introducing the Gibbs phenomenon, which says the partial sum of a Fourier series of a function with jump discontinuities has large oscillations near the jump. Therefore one can reduce the Gibbs phenomenon by choosing a window function whose multipoles higher than the truncation point are suppressed. The author uses a Gaussian smoothing kernel to smooth the edge of the window function whose expression is

$$
W_i = \begin{cases} \displaystyle\int_{-\infty}^{\delta_i - \frac{\delta_c}{2}} \dfrac{1}{\sqrt{2\pi\sigma^2}}\exp\left(-\dfrac{x^2}{2\sigma^2}\right)dx = \dfrac{1}{2} + \dfrac{1}{2}\mathrm{erf}\left(\dfrac{\delta_i - \frac{\delta_c}{2}}{\sqrt{2}\sigma}\right) & \delta_i < \delta_c, \\ 1 & \delta_i > \delta_c, \end{cases} \tag{27}
$$
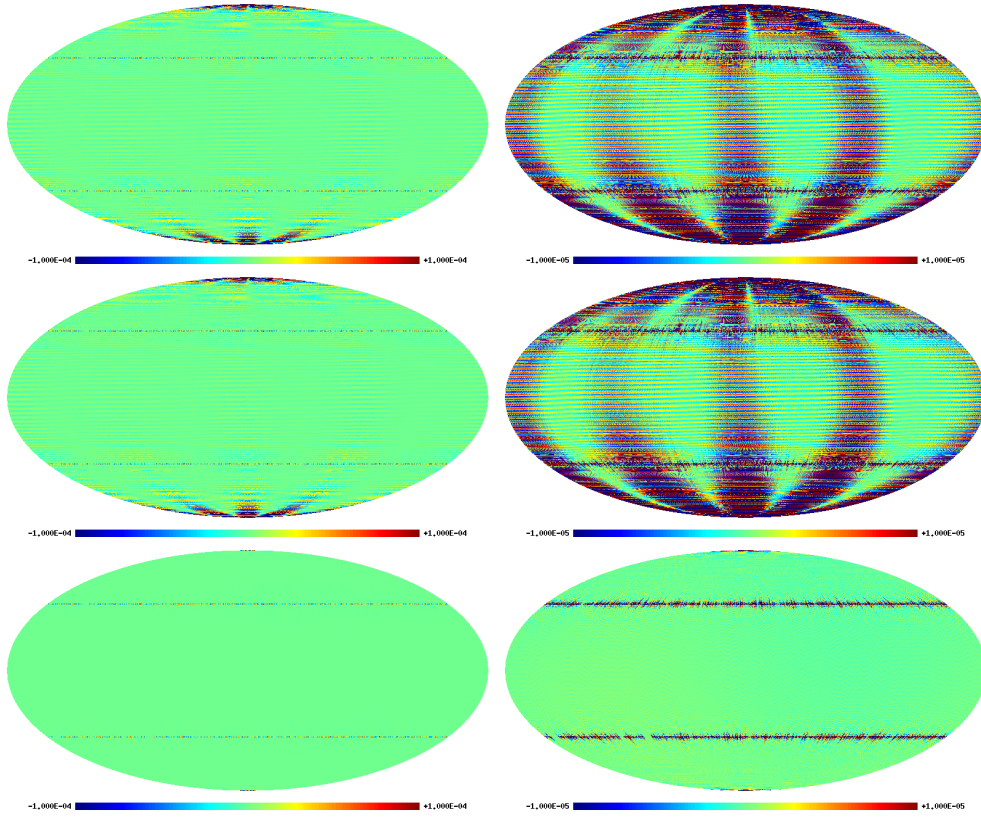
Fig. 5 The pure B-mode field constructed by the SZ method and cos-, sin- and *Gaussian*-smoothing window functions, from top to bottom, respectively, where $\delta_c = 1°$ and $\beta = 10^{-4}$. The panels on the right side have the scaling magnified in order to show the residual leakage.
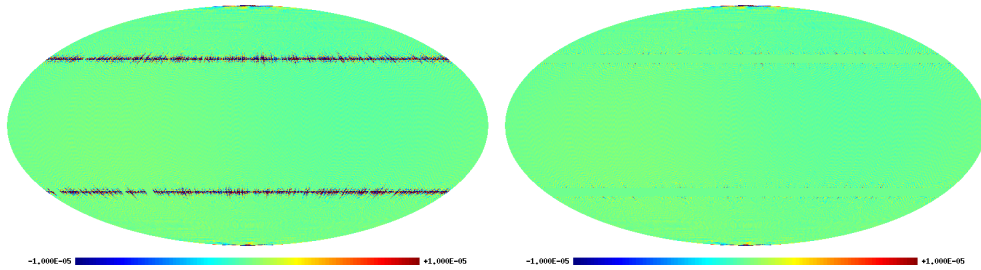
Fig. 6 The pure B-mode field constructed by the SZ method with a *Gaussian*-smoothed window function. The contamination bands have been masked out in the right panel, but in the left one they have not been masked out. These are plotted on the same scale.

where $\sigma = \frac{\text{FWHM}}{\sqrt{8\ln 2}}$ and FWHM denotes the full width at half maximum of the smoothing kernel. Let β denote the jump range at $\delta_i = \delta_c$ and $\delta_i = 0$, then

$$\beta = \frac{1}{2} - \frac{1}{2}\text{erf}\left(\frac{\frac{\delta_c}{2}}{\sqrt{2}\sigma}\right). \tag{28}$$

The β is a small and adjustable parameter. Set $\delta_c = 1°$ and let $\beta = 10^{-4}$ and 10^{-6}. Separate plots of the values of Equations (25), (26) and (27) are given in Figure 2.

Inspired by the explanation of the Gibbs phenomenon, we also analyze the smoothed window functions in harmonic space. We apply cos-smoothing, sin-smoothing and *Gaussian*-smoothing to the top-hat window function, then

decompose the smoothed window function $W(\hat{n})$ (shown in Fig. 2) on the spherical harmonic basis and define the power spectrum W_l as follows

$$W_l = \frac{1}{2l+1}\sum_m w_{lm}w_{lm}^*, \tag{29}$$

where

$$w_{lm} = \int d\hat{n} W(\hat{n}) Y_{lm}^*(\hat{n}). \tag{30}$$

The power spectrum of the smoothed window function using cos, sin and *Gaussian* methods with different parameters is shown as Figure 4. We can see from the figure that the *Gaussian*-smoothed window function has a lower power spectrum on a small scale.
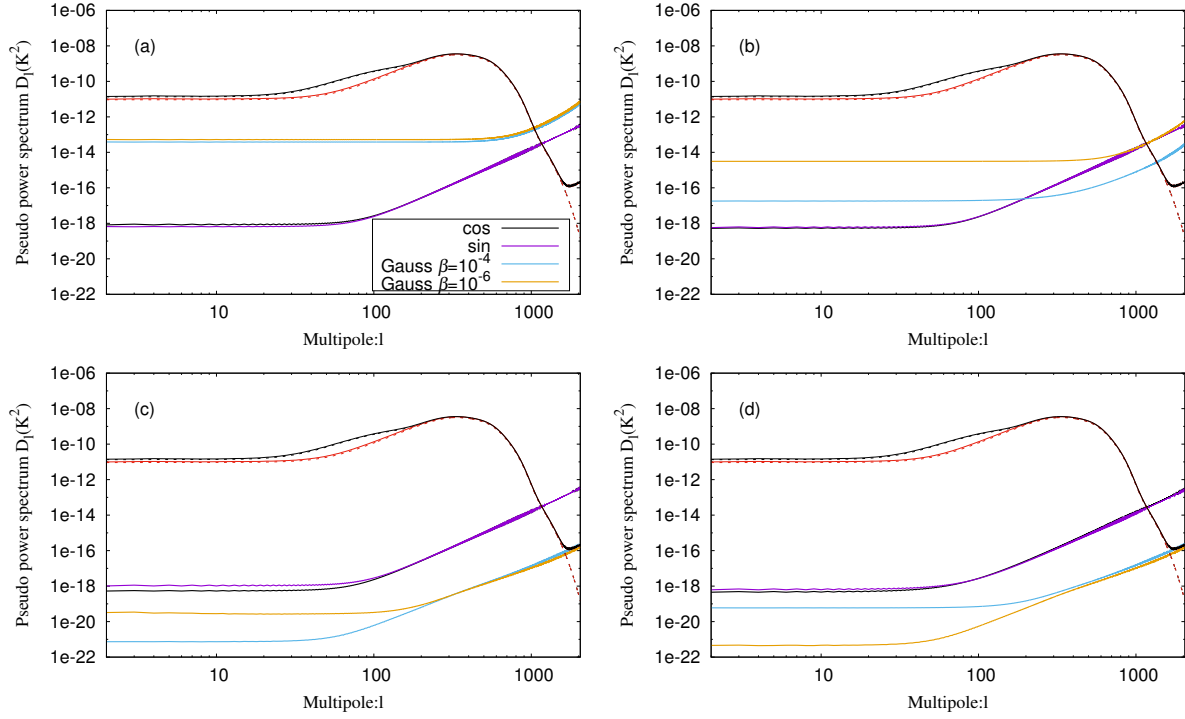
Fig. 7 The pseudo power spectrum of $\mathcal{B}^{\mathrm{pure}}(\hat{n})$ obtained using different smoothed window functions. (a) $\delta_c = 0.2°$; (b) $\delta_c = 0.5°$; (c) $\delta_c = 1.0°$; (d) $\delta_c = 1.5°$. We also plot the power spectrum with signal, using the smoothed mask with $\delta_c = 1.0°$ and $\beta = 10^{-4}$, which are the theoretical power spectrum with $r = 0.1$ (*black dashed line*) and $r = 0$ (*red dashed line*), and the average power spectrum of 1000 simulations with $r = 0.1$ (*black solid line*) and $r = 0$ (*red solid line*). All of the four extra lines include the contribution of cosmic lensing.

We shall investigate the numerical error due to finite pixelization in E- and B-mode separation through simulated polarization maps. We first use the *synfast* subroutine in the HEALPix software package to generate the full sky $Q(\hat{n})$ and $U(\hat{n})$ maps with the best-fit cosmological parameters published by Planck 2013:

$$\Omega_b h^2 = 0.022068, \qquad \Omega_c h^2 = 0.12029,$$
$$\Omega_\Lambda = 0.6825, \qquad \tau_{\mathrm{reion}} = 0.0925, \qquad (31)$$
$$A_s = 2.215 \times 10^{-9}, \qquad n_s = 0.9624.$$

We set the resolution of simulated maps to be $N_{\mathrm{side}} = 1024$ and a Gaussian beam with $\theta_F = 30'$. Assuming there is neither contribution from gravitational waves nor cosmic lensing, i.e. $C_l^{BB} = 0$ in the input model, we use the SZ method and a specific smoothed window function to construct the pure B-mode field as

$$\mathcal{B}^{\mathrm{pure}}(\hat{n}) = \sum_{lm} \mathcal{B}_{lm}^{\mathrm{pure}} Y_{lm}(\hat{n}), \qquad (32)$$

where the expression of $\mathcal{B}_{lm}^{\mathrm{pure}}$ is shown in Equation (22). The $\mathcal{B}^{\mathrm{pure}}(\hat{n})$ is related to $\mathcal{B}(\hat{n})$ in Equation (9) by

$$\mathcal{B}^{\mathrm{pure}}(\hat{n}) = \mathcal{B}(\hat{n})W(\hat{n}). \qquad (33)$$

Figure 5 is a visualization of $\mathcal{B}^{\mathrm{pure}}(\hat{n})$. Since we assume $C_l^{BB} = 0$, all the non-zero value pixels in Figure 5 are attributed to numerical error.

Interestingly enough, the third panel in Figure 5 shows that the numerical errors are mostly concentrated in two bands, due to the design of the HEALPix software package. The HEALPix package divides the sky into three parts, and reassembles them after applying the operation, so there will be some residuals on the resulting joint. Besides, due to this kind of residual located in two narrow bands, we can mask them out to remove most of the contamination with little information being lost.

In Figure 6, we mask out two bands centered at $48°$ and $132°$ and the width of each band is $6°$, then the map looks much cleaner. How to quantify this further reduction of numerical errors in the constructed pure B-mode map is another important topic in this area, so we leave it as future work.

In order to quantify the numerical errors of a pure B-mode map in harmonic space, we define the pseudo power spectrum as

$$D_l^{\mathrm{pure}} = \frac{1}{2l+1} \sum_m \mathcal{B}_{lm}^{\mathrm{pure}} \mathcal{B}_{lm}^{\mathrm{pure}*}. \qquad (34)$$

We use the Monte Carlo method to investigate the effect on numerical errors using different smoothed window functions. The result is shown in Figure 7. Each line is an average over 500 realizations with the same cosmological initial conditions but different random seeds. To compare the magnitude of the signal with numerical error, we also plot the theoretical pseudo power spectrum (see eq. (38) in

Zhao & Baskaran 2010) and the average power spectrum of 1000 simulations with initial condition $r = 0$ and $r = 0.1$ (r is the primordial tensor-to-scalar ratio) respectively and all with the contribution of cosmic lensing.

In Figure 7, for $\mathcal{B}^{\mathrm{pure}}(\hat{n})$ with initial conditions $C_l^{BB} = 0$, all the non-zero values of pseudo power spectra are due to numerical error. Therefore, it can be used to quantitatively measure the intensity of contamination. We can recognize that the tendency of the pseudo power spectrum brought by different smoothed window functions in Figure 7 is almost the same as Figure 4, which means the smoothed window function with smaller multipole values in harmonic space will yield smaller numerical error in E- and B-mode separation. We obtain the results: If δ_c is small, i.e. there is less information loss, sin- and cos-smoothing methods are better than the *Gaussian*-smoothing method. On the other hand, if we need a cleaner map, where δ_c should be larger (such as $\delta_c = 1°$ or $1.5°$), *Gaussian*-smoothing method is better. These can be understood in the following way: comparing with the sin- or cos-smoothing functions, the *Gaussian*-smoothing function is much steeper. So when δ_c is smaller, the *Gaussian* function becomes close to a top-hat function, which will yield a larger numerical error. However, when δ_c is larger (i.e. $\delta_c > 1°$), all these three smoothing functions become relatively flat. However, the *Gaussian*-smoothing function is continuous for any order derivatives around the boundaries, so the numerical errors can be dramatically reduced in the numerical calculations. This can also explain why the leakage residuals in the constructed B-mode map are quite small when the *Gaussian*-smoothing function is adopted (see Fig. 5).

4 CONCLUSIONS

Detection of B-mode polarization is the main aim of future CMB observations. During the real analysis, an incomplete sky survey induces a mixture of the E-mode and B-mode. In order to separate the E- and B-mode of CMB on an incomplete sky, we need to smooth the edge of the window function. In this article we present a comparison of the effects on numerical errors brought by different smoothing methods of the window function. We found that the *Gaussian*-smoothing method with large δ_c results in a cleaner map, but also more information loss, while sin- and cos-smoothing methods do better when δ_c is small, i.e. there is less information loss.

References

Ade, P. A. R., Akiba, Y., Anthony, A. E., et al. 2014, Physical Review Letters, 112, 131302

BICEP2/Keck and Planck Collaborations, Ade, P. A. R., Aghanim, N., et al. 2015, Physical Review Letters, 114, 101301

Bock, J., Church, S., Devlin, M., et al. 2006, astro-ph/0604101

Bunn, E. F. 2008, arXiv:0811.0111

Bunn, E. F., Zaldarriaga, M., Tegmark, M., & de Oliveira-Costa, A. 2003, Phys. Rev. D, 67, 023501

Cao, L., & Fang, L.-Z. 2009, ApJ, 706, 1545

Doroshkevich, A. G., Naselsky, P. D., Verkhodanov, O. V., et al. 2005, International Journal of Modern Physics D, 14, 275

Efstathiou, G. 2004, MNRAS, 349, 603

Ferté, A., Grain, J., Tristram, M., & Stompor, R. 2013, Phys. Rev. D, 88, 023524

Geller, D., Hansen, F. K., Marinucci, D., Kerkyacharian, G., & Picard, D. 2008, Phys. Rev. D, 78, 123533

Górski, K. M., Hivon, E., Banday, A. J., et al. 2005, ApJ, 622, 759

Grain, J., Tristram, M., & Stompor, R. 2009, Phys. Rev. D, 79, 123515

Hanson, D., Hoover, S., Crites, A., et al. 2013, Physical Review Letters, 111, 141301

Kamionkowski, M., Kosowsky, A., & Stebbins, A. 1997a, Physical Review Letters, 78, 2058

Kamionkowski, M., Kosowsky, A., & Stebbins, A. 1997b, Phys. Rev. D, 55, 7368

Kim, J. 2011, A&A, 531, A32

Kim, J., & Naselsky, P. 2010, A&A, 519, A104

Lewis, A. 2003, Phys. Rev. D, 68, 083509

Lewis, A., Challinor, A., & Turok, N. 2002, Phys. Rev. D, 65, 023505

Naess, S., Hasselfield, M., McMahon, J., et al. 2014, J. Cosmol. Astropart. Phys., 10, 7

Planck Collaboration, Aghanim, N., Arnaud, M., et al. 2015, arXiv:1507.02704

Seljak, U., & Zaldarriaga, M. 1997, Physical Review Letters, 78, 2054

Smith, K. M. 2006, Phys. Rev. D, 74, 083002

Smith, K. M., & Zaldarriaga, M. 2007, Phys. Rev. D, 76, 043001

Zaldarriaga, M., & Seljak, U. 1997, Phys. Rev. D, 55, 1830

Zhao, W., & Baskaran, D. 2010, Phys. Rev. D, 82, 023001